Title
Neutralization of BCL-2/XL Enhances the Cytotoxicity of T-DM1 In Vivo

Journal
Molecular Cancer Therapeutics, 18(6)

ISSN
1535-7163

Authors
Zoeller, Jason J
Vagodny, Aleksandr
Taneja, Krishan
et al.

Publication Date
2019-06-01

DOI
10.1158/1535-7163.mct-18-0743

Peer reviewed

HHS Public Access

Author manuscript

Mol Cancer Ther. Author manuscript; available in PMC 2019 December 01.

Published in final edited form as:

Mol Cancer Ther. 2019 June ; 18(6): 1115–1126. doi:10.1158/1535-7163.MCT-18-0743.

Neutralization of BCL-2/X_L enhances the cytotoxicity of T-DM1 *in vivo*

Jason J. Zoeller[1], **Aleksandr Vagodny**[1], **Krishan Taneja**[2], **Benjamin Y. Tan**[2], **Neil O'Brien**[3], **Dennis J. Slamon**[3], **Deepak Sampath**[4], **Joel D. Leverson**[5], **Roderick T. Bronson**[6], **Deborah A. Dillon**[2], **Joan S. Brugge**[1]

[1]Department of Cell Biology and Ludwig Center at Harvard, Harvard Medical School, Boston, MA

[2]Department of Pathology, Brigham & Women's Hospital, Boston, MA

[3]Department of Medicine, David Geffen School of Medicine at UCLA, Los Angeles, CA

[4]Translational Oncology, Genentech, San Francisco, CA

[5]Oncology Development, AbbVie, North Chicago, IL

[6]Department of Pathology, Harvard Medical School, Boston, MA

Abstract

One of the most recent advances in the treatment of HER2+ breast cancer is the development of the antibody-drug conjugate, T-DM1. T-DM1 has proven clinical benefits for patients with advanced and/or metastatic breast cancer who have progressed on prior HER2-targeted therapies. However, T-DM1 resistance ultimately occurs and represents a major obstacle in the effective treatment of this disease. Since anti-apoptotic BCL-2 family proteins can affect the threshold for induction of apoptosis and thus limit the effectiveness of the chemotherapeutic payload, we examined whether inhibition of BCL-2/X_L would enhance the efficacy of T-DM1 in five HER2-expressing patient-derived breast cancer xenograft models. Inhibition of BCL-2/X_L via navitoclax/ABT-263 significantly enhanced the cytotoxicity of T-DM1 in two of three models derived from advanced and treatment-exposed metastatic breast tumors. No additive effects of combined treatment were observed in the third metastatic tumor model which was highly sensitive to T-DM1, as well as a primary treatment-exposed tumor, which was refractory to T-DM1. A fifth model, derived from a treatment naïve primary breast tumor, was sensitive to T-DM1 but markedly benefited from combination treatment. Notably, both PDXs that were highly responsive to the combination therapy expressed low HER2 protein levels and lacked *ERBB2* amplification, suggesting that BCL-2/X_L inhibition can enhance sensitivity of tumors with low HER2 expression. Toxicities associated with combined treatments were significantly ameliorated with intermittent ABT-263 dosing. Taken together, these studies provide evidence that T-DM1 cytotoxicity could be

Corresponding Author Joan S. Brugge, Ph.D., Department of Cell Biology and Ludwig Center at Harvard, Harvard Medical School, 240 Longwood Avenue, Boston, Massachusetts 02115, (p) 617.432.3974, (f) 617.432.3969, joan_brugge@hms.harvard.edu.

Disclosure of Potential Conflicts of Interest D.S. was an employee of Genentech. J.D.L. is an AbbVie employee and owns stock in the company. D.A.D. serves on the Academic Advisory Board of Oncology Analytics, Inc. J.S.B. served as an ad hoc advisor for Oncology program review at Roche Pharmaceuticals in 2018 and Discovery Oncology program review at Genentech in 2017, and received an honorarium for each. The remaining authors have no potential conflicts of interest.

significantly enhanced via BCL-2/X_L blockade and support clinical investigation of this combination beyond *ERBB2*-amplified and/or HER2-overexpressed tumors.

Keywords

BCL-2; BCL-X_L; ABT-263; apoptosis; HER2; ADC; T-DM1; Cytotoxic; Breast; PDX

Introduction

BCL-2 and BCL-X_L pro-survival proteins represent a barrier to effective tumor cell killing by cancer therapies. Agents that neutralize BCL-2 and BCL-X_L (ABT-263/navitoclax) or BCL-2 only (ABT-199/venetoclax) have been developed (1) and provide one approach to target and inhibit the pro-survival function of these proteins (2,3). In preclinical studies, ABT-263 was found to display remarkable enhancement of cell killing by targeted therapies (4–6) and chemotherapies (7–9), and the clinical benefit in solid tumors is currently under investigation in several clinical trials (10). However, treatments combining chemotherapeutic drugs (e.g., carboplatin/paclitaxel) with ABT-263 caused dose-limiting toxicities in patients due to the combined toxicity to platelets and other hematopoietic cells (11). To avoid these systemic side effects and enable the delivery of powerful combinations of chemotherapeutic drugs with BCL-2 family inhibitors, we explored a strategy that combines ABT-263 with an antibody-drug conjugate (ADC). Antibody-drug conjugates link target-specific antibodies to a powerful cytotoxic payload (12). To date, four ADCs are FDA-approved for clinical usage in certain lymphomas (brentuximab vedotin), acute lymphoblastic leukemia (inotuzumab ozogamicin), acute myeloid leukemia (gemtuzumab ozogamicin) or HER2+ breast cancers (trastuzumab emtansine/T-DM1). T-DM1 significantly reduces toxicity to healthy tissues and hematopoietic cells by specifically targeting the delivery of a cytotoxic drug (emtansine; DM1) to HER2+ tumor cells.

T-DM1 combines the anti-HER2 properties of trastuzumab with the anti-microtubule cytotoxic activities of DM1 (13–15). Although the effectiveness and benefits of T-DM1 as second-line or beyond treatment in patients with HER2+ advanced or metastatic breast cancer has been demonstrated in numerous clinical trials (16–22), drug resistance is an eventual occurrence in the majority of patients.

Several lines of evidence indicate that the BCL-2 pro-survival protein prevents drug-induced apoptosis and contributes to HER2-targeted drug resistance. For example, an increased BCL-2:BAX ratio was associated with acquired trastuzumab resistance in one model (23) and BCL-2 up-regulation was shown to be a component of acquired lapatinib resistance in two different models (24,25). Furthermore, there is substantial evidence in the literature that implicates BCL-2/X_L in resistance to chemotherapeutics (26–29). These observations as well as previous studies from our lab and others indicate that BCL-2/X_L inhibitors significantly enhance the efficacy of other therapies by lowering the threshold for apoptosis (1,5,6,8,30–33). As such, we were motivated to examine whether BCL-2/X_L inhibition could improve the efficacy of T-DM1. For these studies, we used HER2-expressing patient-derived xenografts (PDX) transplanted orthotopically into the mouse mammary gland (34,35).

Compared to tumor cell lines, these PDXs recapitulate the heterogeneity, microenvironment and drug responsiveness of human breast tumors.

Materials and Methods

Orthotopic tumor fragment transplantation

Orthotopic tumor fragment transplants were performed as previously described (36). Tumor fragments derived from PDX8 and PDX12 were kindly provided by Alana Welm (Huntsman Cancer Institute) (34). Tumor fragments derived from BCM-3963, BCM-4888 and BCM-3613 were kindly provided by Michael Lewis (Baylor College of Medicine) (35). Briefly, tumor fragments were successfully generated and serially passaged via orthotopic transplant into the mammary fat pad of 6–10 week old female NOD/scid mice. A slow-release estrogen pellet (Innovative Research of America NE-121 0.18 mg 90 days) was implanted subcutaneously to maintain the HER2+ ER+ BCM-4888 model (35). All procedures were carried out according to IACUC 04004 and Harvard ARCM policies.

Drug treatment *in vivo*

For *in vivo* studies, T-DM1 (Genentech) was administered i.p. at 10 mg/kg once per week. ABT-737 (AbbVie) was administered i.p. at 70 mg/kg once per day. ABT-263 (AbbVie) was administered p.o. at 70 mg/kg once per day. T-DM1 was prepared according to Genentech recommendations in sterile water for injection (Gibco). ABT-737 and ABT-263 were prepared according to AbbVie recommendations. ABT-737 in 30% propylene glycol (Sigma) plus 0.5% Tween 80 (Sigma) and 65% D5W (5% dextrose in water, Sigma) pH 3–4 and ABT-263 in 60% PHOSAL 50 PG (Lipoid) plus 30% polyethylene glycol 400 (Dow Chemical) and 10% ethanol. Matched control animals received vehicle alone in the same manner as drug-treated counterparts. All animals were randomized into groups and weighed before treatment. Individual weights were used for dose calculations. Weights were re-measured at the 14-day experimental end point. Weight reductions >20% prevented continuous treatments beyond 14 days.

Bio-specimen collection

Retro-orbital blood collection was performed at the experimental endpoint. Mouse platelet counts were measured by Charles River Research Animal Diagnostic Services (Wilmington, MA). Tumor tissue was harvested at the experimental endpoint and fixed in 10% neutral buffered formalin (Sigma).

Tumor histology, FISH and IHC assays

Tissue was processed for paraffin embedding, sectioning, H&E and trichrome staining by the Harvard Rodent Histopathology Core (Boston, MA). Unstained sections were analyzed by immunohistochemical analysis according to previously described procedures (31). Marker specifics are as follows: HER2 (Dako A0485), HER3 (Cell Signaling Technologies 12708), BCL-2 (Dako M0887), BCL-X_L (Cell Signaling Technologies 2764), EMA (Dako M0613), MCL-1 (Ventana SP143) and p63 (Biocare CM163A). Additional details are summarized in Supplementary Table 1. For BCL-2 and BCL-X_L IHC assays, human tonsil was used as a positive control and un-related PDX tumor tissue was used as a negative

control (incubation with secondary antibody alone). Trichrome results were scored by rodent pathologist Dr. Roderick Bronson as a percentage (0–100) of trichrome-positive stroma present within the tumor cross-sections. IHC results were scored by breast pathologist Dr. Deborah Dillon according to H-scores as previously described (37). Intensities were qualitatively scored as strong (3+), moderate (2+), weak (1+) or negative (0).

$$\mathbf{H-score} = (\%\ \mathbf{of\ cells\ 3+} \times \mathbf{3}) + (\%\ \mathbf{of\ cells\ 2+} \times \mathbf{2}) + (\%\ \mathbf{of\ cells\ 1+} \times \mathbf{1}) + (\%\ \mathbf{of\ cells\ 0} \times \mathbf{0})$$

Unstained sections were evaluated for MCL-1 via IHC on a Ventana Benchmark XT (10 μg per ml antibody, 32 minutes, 37°C). Slides were pre-treated with CC1 mild conditioning and were developed with OptiView DAB for 8 minutes. MCL-1 results were interpreted by pathologist Dr. Franklin Peale according to a qualitative scale of weak, moderate and strong intensity using A549 (very weak), LP1(weak) and MCF7 (moderate to strong) cell line samples for controls. Bacterial artificial chromosome clones RP11–62N23, RP11–1065L22 and RP11–1044P23 were obtained from Children's Hospital Oakland and used in construction of FISH probes for a 340 kb region including *ERBB2*. Probes were biotin-labeled using the Random Prime DNA Labeling System (Invitrogen) according to the manufacturer's protocol and detected with rhodamine (red). The FITC-labeled probe (green) for the chromosome 17 centromeric region was purchased from Abbott/Vysis. Specificity of probe binding was verified using normal lymphocyte metaphase spreads. Dual color FISH was performed on whole tissue sections. Slides were counterstained with DAPI/Antifade (Vector Labs) and evaluated using an Olympus BX51 fluorescence microscope. Hybridization signals were scored by K.T. and D.D. in at least 20 tumor cells according to current ASCO/CAP guidelines (38).

Analysis of treatment effects

Treatment effects, as measured by pathological response, included tumor cross-sectional area and tumor viable cellular content. Both parameters are components of the clinically relevant Residual Cancer Burden score system (39). Tumor cross-sectional area was either approximated with breast pathologist Dr. Deborah Dillon from the H&E sections or approximated via *ex vivo* caliper measurements at the experimental endpoint. Tumor cross-sectional area was based upon estimates of the tumor dimensions (length and width) and calculated by π× ½[length] × ½[width]. Tumor viable cellular content was also approximated with breast pathologist Dr. Deborah Dillon and inferred from the H&E sections. Tumor cell content was scored as a percentage (0–100) of viable invasive carcinoma (IC) present within the tumor cross-sections (intraductal carcinoma (ID) and other cell types were excluded from these estimates).

Microscopy

H&E and IHC images were captured on the laboratory Nikon Eclipse E200 microscope equipped with an Idea color camera and the SPOT software package. H&E and IHC images were scanned, at the Neurobiology Imaging Facility at Harvard Medical School, on the Olympus VS120-S5 microscope equipped with a Hamamatsu ORCA-R2 color camera. The VS-ASW-FL software package was used for image analysis.

Statistics

Statistical analyses were performed using GraphPad Prism version 7 for MAC. For the analysis of continuous variables with normal distributions, Welch's *t* test was applied. For the analysis of non-normal data, Mann-Whitney test was applied.

Results

Characterization of PDX models

Five HER2-expressing PDXs (Table 1) (34,35) were established in female NOD/scid mice via orthotopic transplantation of tumor fragments as described previously (36). Two models were derived from patient primary breast tumors (35). BCM-3963 was established before the patient received treatment (treatment naïve) whereas BCM-4888 was established after the patient received treatment. Three models (PDX12, PDX8 and BCM-3613) were established from pleural effusions after the patients received systemic treatment with numerous HER2-targeted and/or standard chemotherapeutics (34,35). As such, the latter models recapitulate advanced and metastatic human breast cancer.

To compare HER2 protein levels, we analyzed the expression of HER2 by IHC (Fig. 1f–j). The levels of these proteins, as summarized in Table 1, were quantified via intensity score assessment as previously described (38). HER2 IHC (using the FDA-approved HER2 antibody A0485, which recognizes an intracellular epitope) indicated that BCM-3613 (IHC 3+) and BCM-3963 (IHC 3+) expressed the highest levels of HER2. PDX8 (IHC 2+) and BCM-4888 (IHC 2+) expressed moderate levels while PDX12 expressed the lowest levels of HER2 overall (IHC 1+). To assess HER2 amplification in these models, we carried out FISH analysis. The three BCM PDX models were positive for *ERBB2* amplification (Supplementary Fig. 1); however, PDX12 and PDX8 lacked *ERBB2* amplification (Supplementary Fig. 1).

Review of the clinical records and pathology reports for PDX8 and PDX12 and comparison to the IHC and FISH analyses of the PDX models indicated that the HER2 levels changed after the initial HER2 diagnosis. With respect to PDX8, the patient's primary breast tumor was described as HER2-positive (IHC 3+) whereas the pleural cells from which PDX8 were derived, were recorded as weak HER2-positive. Interestingly, for PDX12, the patient's primary breast tumor was initially described as HER2-negative (IHC 1+) ER/PR-positive, whereas the first recurrence was described as HER2-positive, ER/PR-negative.

We also analyzed the expression levels of BCL-2 (Fig. 1k–o) and BCL-X_L (Fig. 1p–t) by IHC and quantified via H-score assessment (37). PDX12, PDX8, BCM-3963 and BCM-3613 tumors expressed overall moderate levels of BCL-X_L (Table 1) and, consistent with an ER-negative phenotype (34,35), undetectable levels of BCL-2 (Table 1) (40–42). BCM-4888 tumors (35) expressed moderate levels of BCL-X_L and low levels of BCL-2, unlike the majority of ER+ tumors, which express high BCL-2 (40–42) (Table 1). For comparative purposes, this information is summarized in Table 1.

Analysis of treatment effects

We initiated our pre-clinical treatment studies using PDX12 and PDX8. Following tumor establishment, tumor-bearing mice (n = 3–5 mice per group) were randomized into one of four treatment arms: T-DM1, ABT-263, T-DM1 + ABT-263 or vehicles (Supplementary Fig. 2). T-DM1 was administered at 10 mg/kg i.p. once per week. ABT-263 was administered at 70 mg/kg p.o. once per day for 14 days. Vehicle controls were administered in the same manner and schedule. To explore alternative dosing schedules that could alleviate known adverse events such as thrombocytopenia, which has been shown to be associated with T-DM1 (43) and ABT-263 (44,45) monotherapy, we included a fifth treatment arm designated T-DM1 + ^{PULSE}ABT-263. These animals received intermittent (pulse) ABT-263 treatments administered at 70 mg/kg p.o. on days 2–4 on each of two successive seven day periods. Continuous combination treatment was associated with weight loss and thrombocytopenia but pulse combination treatment did not elicit either of these side effects (Supplementary Fig. 2).

Microscopic analysis of the PDX12 tumor H&E sections revealed that single agent T-DM1 or ABT-263 treatment had minimal effects on the invasive tumor cells; however, combination treatment resulted in substantial elimination of the tumor cells and the emergence of a reactive stromal-rich tumor bed (Fig. 2). We found similar combination effectiveness in PDX8. PDX8 tumors, which are smaller in size than PDX12 tumors, exhibited partial responses to single agent T-DM1. This response was dramatically enhanced with ABT-263 treatment (Fig. 2).

To better distinguish tumor cells from stromal elements, we used epithelial membrane antigen (EMA) IHC to visualize tumor cells and trichrome stain to visualize stromal content (Fig. 3). Consistent with our H&E observations and quantitative measurements, the combination of T-DM1 and ABT-263, decreased EMA+ content (tumor) and increased trichrome+ content (stroma) when compared to each agent alone. The quantitative pathological assessment of viable tumor cell content for each tumor, which is based on the proportion of viable invasive, non-intraductal, carcinoma present within the tumor cross-sections (Fig. 4a and 4d), demonstrates a significant reduction in neoplastic tumor cell content with combined T-DM1 and ABT-263 treatment in both models. Quantitative pathological assessment of tumor stroma, which is based on the proportion of trichrome+ content present within the tumor cross-sections (Fig. 4b and 4e), further supports the significant reduction in neoplastic tumor cell content and the emergence of a reactive stromal-rich tumor bed in response to combined T-DM1 and continuous ABT-263 treatment in both models.

We also examined the cross-sectional area of the tumors, which reflects the overall size of the tumors post-treatment, and consists of both tumor and stromal components. The cross-sectional areas of PDX12 combination-treated tumors were significantly reduced at the experimental endpoint compared to T-DM1-treated tumors (Fig. 4c and Supplementary Fig. 3A). Despite the significant reduction in tumor cell content (Fig. 4d), the combination treatment effect on the cross-sectional areas of the much smaller PDX8 tumors, which were sensitive to T-DM1 alone, was less significant (Fig. 4f and Supplementary Fig. 3A). Due to the small size and the stromal infiltration associated with reduction in tumor cell content, the

cross-sectional tumor area doesn't accurately reflect the effects of drug treatment on PDX8 whereas closer inspection of tumor cell and stromal content does (Fig. 3). Comparison of the combination treatments with either continuous or pulsatile ABT-263 revealed that there were no statistically significant differences in the reduction of either tumor cell content or cross sectional area between the two dosing schedules for PDX8 (Fig. 4a and 4c) or PDX12 (Fig. 4d and 4f).

PDX12 tumors were treated with T-DM1 + continuous dosing of ABT-737, a derivative of ABT-263 that also neutralizes BCL-2/X_L, to determine whether this agent mimicked the efficacy observed with T-DM1 + ABT-263 (Supplementary Fig. 4). Combination-treated PDX12 tumors were characterized by significantly reduced cross-sectional area and tumor cell content (Supplementary Fig. 4). For PDX8, three out of five PDX8 tumors treated with T-DM1 + ABT-737 displayed a dramatic reduction in tumor cell content with significant stromal cell infiltration, similar to the T-DM1 + ABT-263 response. The reduction in cross sectional areas of the combination treated tumors were similar to those of T-DM1, as observed with ABT-263 + T-DM1 combinations (Supplementary Fig. 4).

We next tested the T-DM1 + ABT-263 combination treatment in the three additional HER2-expressing PDX models (BCM-3963, BCM-4888 and BCM-3613). Tumor-bearing mice were randomized into four groups as described above. ABT-263 was administered continuously with an experimental endpoint on day 14. Treatment-naïve BCM-3963 was sensitive to single agent T-DM1 (Fig. 5a–d and Supplementary Fig. 3B). Consistent with this, the patient from which this xenograft was derived responded to trastuzumab and lapatinib and the initially established BCM-3963 xenografts were reported to be sensitive to trastuzumab and lapatinib (35). Calculation of tumor cross-sectional area indicated that combination treatment was comparable to single agent T-DM1 in reducing tumor size (Fig. 5e). However, specific analysis of the residual tumor cell mass indicated that a significant portion of the residual mass was stromal cells, thus indicating that the addition of ABT-263 enhanced T-DM1 cytotoxicity (Fig. 5f). BCM-4888 was insensitive to single agent T-DM1 but partially sensitive to single agent ABT-263 treatment (Fig. 5g–l and Supplementary Fig. 3B). Assessment of viable tumor cell content indicated that the combination treatment was comparable to single agent ABT-263 (Fig. 5l). Combination treatment benefits were not observed within BCM-3613 tumors, which were highly sensitive to single agent T-DM1 (Fig. 5m–r and Supplementary Fig. 3B).

Analysis of residual tumor cells

Under all treatment conditions examined, islands of residual EMA+ tumor cells were observed in PDX12 and PDX8. These were scattered throughout a trichrome+ reactive stroma similar to post-treatment patient samples observed in the clinic (46). Since a subset of residual PDX8 tumor cells exhibited intraductal-like histology, we performed p63 immunohistochemistry in order to label myoepithelial cells which surround the mammary ducts. The majority of the residual PDX8 tumor cells were present within p63+ ducts (Supplementary Fig. 5A). Residual PDX12 tumor cells were not surrounded by myoepithelial cells indicating that they are not intraductal, but rather invasive. These results

suggest that tumor cells within ducts may escape the cytotoxicity of T-DM1 + ABT-263 combined treatment.

Since MCL-1 levels have been shown to correlate with resistance to ABT-263 (47–50), we performed MCL-1 IHC on PDX12 and PDX8 tumors. PDX12 and PDX8 tumors express low levels of MCL-1. We did not detect any enrichment of MCL-1 expression in the residual cells following treatment with T-DM1 + ABT-263, suggesting that enhanced expression of MCL-1 does not associate with lack of sensitivity to the drug combination in PDX12 and PDX8 tumor cells that remain after treatment (Supplementary Fig. 5B).

Since intracellular delivery of T-DM1 depends on the level of target expression, we also evaluated HER2 levels within PDX12 and PDX8 tumors treated with T-DM1 alone or in combination with ABT-263. For HER2 IHC, we used HER2 antibody A0485 and quantification via H-scores (37) in order to detect and compare HER2 across all treatment groups. Decreased total HER2 protein levels were observed in PDX12 and PDX8 tumors treated with T-DM1 alone, in combination with ABT-263 (Fig. 6) or in combination with ABT-737 (Supplementary Fig. 6); however, the effect in PDX12 is subtle because the pre-treatment levels are very low to begin with. Since HER3 has been shown to contribute to T-DM1 resistance (13), HER3 expression was also examined. HER3 levels were unaltered in PDX8 (Supplementary Fig. 5C) and undetectable in PDX12 tumors, suggesting specific reductions in HER2 expression. The same treatments did not alter HER2 protein levels in BCM-3963, BCM-4888 or BCM-3613 tumors (Supplementary Fig. 7). These results suggest that decreased HER2 expression could explain, at least in part, the presence of residual T-DM1-insensitive PDX12 and PDX8 tumor cells. Since some of the residual tumor cells displayed HER2 levels similar to untreated tumor cells, other factors likely contribute to resistance as well. Immunohistochemical evaluation of cell proliferation (Ki67), pro-apoptotic protein levels (BIM) and cell signaling (phospho-S6) did not show distinguishable differences in residual tumor cells between untreated and treated groups. Interestingly, PDX12 tumors treated with ABT-263 (Fig. 6) or ABT-737 (Supplementary Fig. 6) exhibited increased HER2 protein levels. These results suggest that enhanced target expression underscores response to combination treatment in PDX12 tumors.

Discussion

Here, we characterized the *in vivo* responses of five HER2-expressing PDX models to T-DM1 + ABT-263 combination treatment. Neutralization of BCL-2/X_L proteins, in three of the five models, resulted in enhanced T-DM1 cytotoxic treatment effects, as opposed to cytostatic treatment effects, characterized by widespread elimination of the invasive tumor cells. Beyond characterization of treatment efficacy, we determined that pulsatile ABT-263 treatments minimize the reduction of platelets, which is a side effect of both T-DM1 and navitoclax, and largely maintain combination effectiveness in the two models where pulsed delivery was evaluated. Furthermore, we characterized the residual tumor cell populations that escape combination treatment and identified lower expression of HER2 as a potential factor.

The five PDX models that we examined displayed heterogeneous responses to single agent T-DM1 and the T-DM1 + ABT-263 combination treatment. These PDX models recapitulate the heterogeneity of human HER2-expressing breast cancers and highlight relevant clinical scenarios. BCM-3963 represents a treatment-naïve bona fide HER2+ patient primary breast tumor with ultrasensitive responses to HER2-targeted therapies *in vivo* (i.e., trastuzumab, lapatinib, T-DM1) (35). In this model, where single agent HER2 therapy was highly effective, we observed added benefit of ABT-263 based on a further reduction of tumor cell content. PDX12 and PDX8, which were derived from HER2-expressing patient pleural effusions, represent advanced metastatic disease. The PDX12 and PDX8 models exhibited partial responses to T-DM1 single agent but dramatic and near complete responses to combination treatment. Assessment of HER2 levels in established PDX12 and PDX8 tumors indicated that these tumors expressed low levels of HER2 and lacked *ERBB2* amplification. It has previously been reported that HER2 expression can decrease throughout patient disease progression (51,52) and that loss of HER2 can occur in response to clinical treatment (53–59). Nonetheless, the ability of ABT-263 to dramatically enhance tumor cell killing in both of these models highlights the potential relevance of this drug combination to patients with advanced and/or metastatic breast cancer who have progressed on the standard-of-care first-line and second-line treatments. Furthermore, T-DM1 effectiveness in the low-HER2 tumors extends consideration and application of this drug combination and concept outside of *ERBB2*-amplified and/or HER2-overexpressed breast cancers.

Two models failed to show enhanced responsiveness to the drug combination relative to single agents. BCM-3613 was derived from a HER2+ patient pleural effusion and is highly sensitive to T-DM1 alone, exhibiting a dramatic reduction in tumor area without evidence of cytoxicity. This suggests that BCM-3613 may have a high threshold for cell death and is thus sensitive to T-DM1-associated proliferative blockade, but not cytotoxic death. BCM-4888 represents a post-treatment HER2+ patient primary breast tumor that is highly refractory to T-DM1. In this model, single agent T-DM1 was ineffective whereas ABT-263 was partially effective. The insensitivity to T-DM1 may limit the extent to which ABT-263 would have additive effects.

One notable finding in the PDX8 model was the detection of residual drug-resistant tumor cells confined within p63+ ductal spaces. This observation remarkably recapitulates the features of residual DCIS often encountered in patient specimens post-treatment within the context of near complete or complete pathological responses (60,61). These findings and previous observations from our lab and others highlight the protected status of tumor cells confined within myoepithelial cells and basement membrane (31).

Another interesting observation from our studies was the finding that HER2 protein levels were lower in tumors treated with T-DM1 alone or in combination with ABT-263. Lower target expression could account, at least in part, for the residual T-DM1 insensitive tumor cells. Unexpectedly, ABT-263 treatment alone upregulated HER2 protein levels in one of the five PDX models we examined (PDX12). This result was confirmed with ABT-737. Although the mechanism that mediates/underlies/regulates this process remains to be determined, the combination effectiveness observed in PDX12 tumors could potentially be

explained by enhanced target expression. Similar upregulation of HER2 and sensitization to T-DM1 has been documented in gemcitabine-treated MCF7 tumor cells (62).

Although MCL-1 has been reported to confer resistance to ABT-263 treatment (47–50), our evidence does not support a role for MCL-1 as a critical component of the residual PDX12 or PDX8 tumor cells. Tumors were overall MCL-1-low, with no evidence of MCL-1 upregulation or of selection of MCL-1-positive cells post-treatment. Consistent with an ER-negative phenotype, both PDX12 and PDX8 tumors expressed low levels of BCL-2 (40–42) but moderate levels of BCL-X_L. As such, we predict combination effectiveness is mediated via BCL-X_L neutralization.

The BCL-2-selective inhibitor venetoclax mitigates thrombocytopenia associated with BCL-X_L inhibition and may represent an attractive agent for treating ER+ tumors, which are enriched for BCL-2 (3,40–42). Indeed pre-clinical data have shown that BCL-2 inhibition in combination with ER blockade is efficacious in HER2-ER+ PDX models (33) and suggests that HER2+ER+ tumors could also benefit from BCL-2-selective blockade in combination with HER2- and ER-targeted therapies.

Despite substantial pre-clinical evidence for the effectiveness of ABT-263/taxol combinations (8), clinical application was not feasible due to side effects of systemic treatment with both drugs (1,11). ADCs, which target and selectively deliver a payload to tumor cells, minimize these potential side effects. One concern regarding combined treatment with T-DM1 and ABT-263 is the potential for dose-limiting thrombocytopenia. ABT-263 treatment depletes mature platelets due to the dependence of these cells on BCL-X_L for survival (63,64). T-DM1 has been shown to be taken up by megakaryocyte platelet precursors and inhibits generation of platelets due to toxicity (65–67). Thus, T-DM1 and ABT-263 have non-overlapping effects on platelets. Although T-DM1-associated platelet side effects were not observed at our experimental endpoints, continuous ABT-263 treatment-associated thrombocytopenia was indeed notable. We circumvented this issue by intermittent dosing of ABT-263, which eliminated thrombocytopenia without significant reduction in efficacy.

Taken together, our pre-clinical studies highlight T-DM1 plus ABT-263 as an effective treatment option worthy of future clinical investigation. The development of next-generation HER2 ADCs (68–72), with proven effectiveness and without platelet liabilities, further support exploration of ABT-263/navitoclax within HER2-expressing breast and other tumor types.

Supplementary Material

Refer to Web version on PubMed Central for supplementary material.

Acknowledgements

We would like to acknowledge Alana Welm, Yoko DeRose (Huntsman Cancer Institute) and Michael Lewis (Baylor College of Medicine) for the PDX tumor models used throughout these studies. We would like to thank Franklin Peale (Genentech Pathology) and Sreedevi Chalasani (Genentech Pathology) for immuno-staining and interpreting the MCL-1 results. We would also like to acknowledge Andrew Thompson (Harvard Pathology) and Li Zhang

(Harvard Pathology) for specialized histological assistance. We would like to thank Angie Martinez Gakidis (Harvard Cell Biology) for critical editing of the manuscript. We would also like to thank Gail Phillips (Genentech) for helpful discussions and critical review of the manuscript. We are grateful for the translational insight provided by Geoffrey Shapiro, Jean Connors and Adrienne Anderson (Dana-Farber Cancer Institute). We are grateful for the patient advocacy provided by Ruth Fax (Dana-Farber Cancer Institute). We would also like to thank the Harvard Medical School Neurobiology Imaging Facility (supported in part by NINDS P30 NS072030) for access to and usage of the slide scanner. Our work was supported by a Developmental Research Project Award, Project Number 9617846 (J.J. Zoeller) awarded through the Dana-Farber Harvard Cancer Center Breast SPORE, Grant Number P50CA168504, and donor funds provided to Dana-Farber by the Sand Dollar Fund, a Stand Up TO Cancer-American Association for Cancer Research Dream Team Translational Cancer Research Grant, Grant Number SU2C-AACR-DT0409 (J.S. Brugge), the Breast Cancer Research Foundation, Grant Number BCRF-16–020 (J.S. Brugge), and a Department of Defense Breast Cancer Research Breakthrough Award, Grant Number W81XWH-16-1-0340 (J.S. Brugge and J.J. Zoeller).

Abbreviations

ADC	antibody-drug conjugate
BCM	Baylor College of Medicine
cape	capecitabine
cyclo	cyclophosamide
DCIS	ductal carcinoma *in situ*
doce	docetaxel
doxo	doxorubicin
EMA	epithelial membrane antigen
ER	estrogen receptor
FDA	Food & Drug Administration
FISH	fluorescence *in situ* hybridization
GSI	gamma secretase inhibitor
H&E	hematoxylin & eosin
HER2	human epidermal growth factor receptor 2
IC	invasive carcinoma
ID	intraductal carcinoma
i.p.	intra-peritoneal
IHC	immunohistochemistry
LN	lymph node
NS	non-significant
pacl	paclitaxel
p.o.	*per os*

PDX	patient-derived xenograft
PE	pleural effusion
PR	progesterone receptor
PT	primary breast tumor
RCB	Residual Cancer Burden
T-DM1	trastuzumab-DM1
T×	treatment
vino	vinorelbine
5-FU	5-fluorouracil

References

1. Leverson JD, Phillips DC, Mitten MJ, Boghaert ER, Diaz D, Tahir SK, et al. Exploiting selective BCL-2 family inhibitors to dissect cell survival dependencies and define improved strategies for cancer therapy. Sci Transl Med 2015;7(279):279ra40 10.1126/scitranslmed.aaa4642.
2. Oltersdorf T, Elmore SW, Shoemaker AR, Armstrong RC, Augeri DJ, Belli BA, et al. An inhibitor of Bcl-2 family proteins induces regression of solid tumours. Nature 2005;435(7042):677–81 10.1038/nature03579. [PubMed: 15902208]
3. Souers AJ, Leverson JD, Boghaert ER, Ackler SL, Catron ND, Chen J, et al. ABT-199, a potent and selective BCL-2 inhibitor, achieves antitumor activity while sparing platelets. Nat Med 2013;19(2): 202–8 10.1038/nm.3048. [PubMed: 23291630]
4. Tan N, Wong M, Nannini MA, Hong R, Lee LB, Price S, et al. Bcl-2/Bcl-xL inhibition increases the efficacy of MEK inhibition alone and in combination with PI3 kinase inhibition in lung and pancreatic tumor models. Mol Cancer Ther 2013;12(6):853–64 10.1158/1535-7163.mct-12-0949. [PubMed: 23475955]
5. Corcoran RB, Cheng KA, Hata AN, Faber AC, Ebi H, Coffee EM, et al. Synthetic lethal interaction of combined BCL-XL and MEK inhibition promotes tumor regressions in KRAS mutant cancer models. Cancer Cell 2013;23(1):121–8 10.1016/j.ccr.2012.11.007. [PubMed: 23245996]
6. Faber AC, Farago AF, Costa C, Dastur A, Gomez-Caraballo M, Robbins R, et al. Assessment of ABT-263 activity across a cancer cell line collection leads to a potent combination therapy for small-cell lung cancer. Proc Natl Acad Sci U S A 2015;112(11):E1288–96 10.1073/pnas. 1411848112. [PubMed: 25737542]
7. Ackler S, Mitten MJ, Foster K, Oleksijew A, Refici M, Tahir SK, et al. The Bcl-2 inhibitor ABT-263 enhances the response of multiple chemotherapeutic regimens in hematologic tumors in vivo. Cancer Chemother Pharmacol 2010;66(5):869–80 10.1007/s00280-009-1232-1. [PubMed: 20099064]
8. Chen J, Jin S, Abraham V, Huang X, Liu B, Mitten MJ, et al. The Bcl-2/Bcl-X(L)/Bcl-w inhibitor, navitoclax, enhances the activity of chemotherapeutic agents in vitro and in vivo. Mol Cancer Ther 2011;10(12):2340–9 10.1158/1535-7163.mct-11-0415. [PubMed: 21914853]
9. Tan N, Malek M, Zha J, Yue P, Kassees R, Berry L, et al. Navitoclax enhances the efficacy of taxanes in non-small cell lung cancer models. Clin Cancer Res 2011;17(6):1394–404 10.1158/1078-0432.ccr-10-2353. [PubMed: 21220478]
10. Cragg MS, Harris C, Strasser A, Scott CL. Unleashing the power of inhibitors of oncogenic kinases through BH3 mimetics. Nat Rev Cancer 2009;9(5):321–6 10.1038/nrc2615. [PubMed: 19343035]
11. Vlahovic G, Karantza V, Wang D, Cosgrove D, Rudersdorf N, Yang J, et al. A phase I safety and pharmacokinetic study of ABT-263 in combination with carboplatin/paclitaxel in the treatment of

patients with solid tumors. Invest New Drugs 2014;32(5):976–84 10.1007/s10637-014-0116-3. [PubMed: 24894650]

12. Govindan SV, Goldenberg DM. Designing immunoconjugates for cancer therapy. Expert Opin Biol Ther 2012;12(7):873–90 10.1517/14712598.2012.685153. [PubMed: 22679911]
13. Phillips GD, Fields CT, Li G, Dowbenko D, Schaefer G, Miller K, et al. Dual targeting of HER2-positive cancer with trastuzumab emtansine and pertuzumab: critical role for neuregulin blockade in antitumor response to combination therapy. Clin Cancer Res 2014;20(2):456–68 10.1158/1078-0432.ccr-13-0358. [PubMed: 24097864]
14. Barok M, Tanner M, Koninki K, Isola J. Trastuzumab-DM1 causes tumour growth inhibition by mitotic catastrophe in trastuzumab-resistant breast cancer cells in vivo. Breast Cancer Res 2011;13(2):R46 10.1186/bcr2868. [PubMed: 21510863]
15. Junttila TT, Li G, Parsons K, Phillips GL, Sliwkowski MX. Trastuzumab-DM1 (T-DM1) retains all the mechanisms of action of trastuzumab and efficiently inhibits growth of lapatinib insensitive breast cancer. Breast Cancer Res Treat 2011;128(2):347–56 10.1007/s10549-010-1090-x. [PubMed: 20730488]
16. Krop IE, Beeram M, Modi S, Jones SF, Holden SN, Yu W, et al. Phase I study of trastuzumab-DM1, an HER2 antibody-drug conjugate, given every 3 weeks to patients with HER2-positive metastatic breast cancer. J Clin Oncol 2010;28(16):2698–704 10.1200/jco.2009.26.2071. [PubMed: 20421541]
17. Burris HA 3rd, Rugo HS, Vukelja SJ, Vogel CL, Borson RA, Limentani S, et al. Phase II study of the antibody drug conjugate trastuzumab-DM1 for the treatment of human epidermal growth factor receptor 2 (HER2)-positive breast cancer after prior HER2-directed therapy. J Clin Oncol 2011;29(4):398–405 10.1200/jco.2010.29.5865. [PubMed: 21172893]
18. Olson EM, Lin NU, DiPiro PJ, Najita JS, Krop IE, Winer EP, et al. Responses to subsequent anti-HER2 therapy after treatment with trastuzumab-DM1 in women with HER2-positive metastatic breast cancer. Ann Oncol 2012;23(1):93–7 10.1093/annonc/mdr061. [PubMed: 21531783]
19. Krop IE, LoRusso P, Miller KD, Modi S, Yardley D, Rodriguez G, et al. A phase II study of trastuzumab emtansine in patients with human epidermal growth factor receptor 2-positive metastatic breast cancer who were previously treated with trastuzumab, lapatinib, an anthracycline, a taxane, and capecitabine. J Clin Oncol 2012;30(26):3234–41 10.1200/jco.2011.40.5902. [PubMed: 22649126]
20. Verma S, Miles D, Gianni L, Krop IE, Welslau M, Baselga J, et al. Trastuzumab emtansine for HER2-positive advanced breast cancer. N Engl J Med 2012;367(19):1783–91 10.1056/NEJMoa1209124. [PubMed: 23020162]
21. Krop IE, Kim SB, Gonzalez-Martin A, LoRusso PM, Ferrero JM, Smitt M, et al. Trastuzumab emtansine versus treatment of physician's choice for pretreated HER2-positive advanced breast cancer (TH3RESA): a randomised, open-label, phase 3 trial. Lancet Oncol 2014;15(7):689–99 10.1016/s1470-2045(14)70178-0. [PubMed: 24793816]
22. Krop IE, Lin NU, Blackwell K, Guardino E, Huober J, Lu M, et al. Trastuzumab emtansine (T-DM1) versus lapatinib plus capecitabine in patients with HER2-positive metastatic breast cancer and central nervous system metastases: a retrospective, exploratory analysis in EMILIAdagger. Ann Oncol 2015;26(1):113–9 10.1093/annonc/mdu486. [PubMed: 25355722]
23. Crawford A, Nahta R. Targeting Bcl-2 in Herceptin-Resistant Breast Cancer Cell Lines. Curr Pharmacogenomics Person Med 2011;9(3):184–90. [PubMed: 22162984]
24. Xia W, Bacus S, Hegde P, Husain I, Strum J, Liu L, et al. A model of acquired autoresistance to a potent ErbB2 tyrosine kinase inhibitor and a therapeutic strategy to prevent its onset in breast cancer. Proc Natl Acad Sci U S A 2006;103(20):7795–800 10.1073/pnas.0602468103. [PubMed: 16682622]
25. Wang YC, Morrison G, Gillihan R, Guo J, Ward RM, Fu X, et al. Different mechanisms for resistance to trastuzumab versus lapatinib in HER2-positive breast cancers--role of estrogen receptor and HER2 reactivation. Breast Cancer Res 2011;13(6):R121 10.1186/bcr3067. [PubMed: 22123186]
26. Miyashita T, Reed JC. Bcl-2 oncoprotein blocks chemotherapy-induced apoptosis in a human leukemia cell line. Blood 1993;81(1):151–7. [PubMed: 8417786]

27. Dole M, Nunez G, Merchant AK, Maybaum J, Rode CK, Bloch CA, et al. Bcl-2 inhibits chemotherapy-induced apoptosis in neuroblastoma. Cancer Res 1994;54(12):3253–9. [PubMed: 8205548]
28. Decaudin D, Geley S, Hirsch T, Castedo M, Marchetti P, Macho A, et al. Bcl-2 and Bcl-XL antagonize the mitochondrial dysfunction preceding nuclear apoptosis induced by chemotherapeutic agents. Cancer Res 1997;57(1):62–7. [PubMed: 8988042]
29. Sartorius UA, Krammer PH. Upregulation of Bcl-2 is involved in the mediation of chemotherapy resistance in human small cell lung cancer cell lines. Int J Cancer 2002;97(5):584–92. [PubMed: 11807782]
30. Muranen T, Selfors LM, Worster DT, Iwanicki MP, Song L, Morales FC, et al. Inhibition of PI3K/mTOR leads to adaptive resistance in matrix-attached cancer cells. Cancer Cell 2012;21(2):227–39 10.1016/j.ccr.2011.12.024. [PubMed: 22340595]
31. Zoeller JJ, Bronson RT, Selfors LM, Mills GB, Brugge JS. Niche-localized tumor cells are protected from HER2-targeted therapy via upregulation of an anti-apoptotic program in vivo. npj Breast Cancer 2017;3(18) 10.1038/s41523-017-0020-z.
32. Oakes SR, Vaillant F, Lim E, Lee L, Breslin K, Feleppa F, et al. Sensitization of BCL-2-expressing breast tumors to chemotherapy by the BH3 mimetic ABT-737. Proc Natl Acad Sci U S A 2012;109(8):2766–71 10.1073/pnas.1104778108. [PubMed: 21768359]
33. Vaillant F, Merino D, Lee L, Breslin K, Pal B, Ritchie ME, et al. Targeting BCL-2 with the BH3 mimetic ABT-199 in estrogen receptor-positive breast cancer. Cancer Cell 2013;24(1):120–9 10.1016/j.ccr.2013.06.002. [PubMed: 23845444]
34. DeRose YS, Wang G, Lin YC, Bernard PS, Buys SS, Ebbert MT, et al. Tumor grafts derived from women with breast cancer authentically reflect tumor pathology, growth, metastasis and disease outcomes. Nat Med 2011;17(11):1514–20 10.1038/nm.2454. [PubMed: 22019887]
35. Zhang X, Claerhout S, Prat A, Dobrolecki LE, Petrovic I, Lai Q, et al. A renewable tissue resource of phenotypically stable, biologically and ethnically diverse, patient-derived human breast cancer xenograft models. Cancer Res 2013;73(15):4885–97 10.1158/0008-5472.can-12-4081. [PubMed: 23737486]
36. DeRose YS, Gligorich KM, Wang G, Georgelas A, Bowman P, Courdy SJ, et al. Patient-derived models of human breast cancer: protocols for in vitro and in vivo applications in tumor biology and translational medicine. Curr Protoc Pharmacol 2013;Chapter 14:Unit14 23 10.1002/0471141755.ph1423s60. [PubMed: 23456611]
37. Goulding H, Pinder S, Cannon P, Pearson D, Nicholson R, Snead D, et al. A new immunohistochemical antibody for the assessment of estrogen receptor status on routine formalin-fixed tissue samples. Hum Pathol 1995;26(3):291–4. [PubMed: 7890280]
38. Wolff AC, Hammond ME, Hicks DG, Dowsett M, McShane LM, Allison KH, et al. Recommendations for human epidermal growth factor receptor 2 testing in breast cancer: American Society of Clinical Oncology/College of American Pathologists clinical practice guideline update. J Clin Oncol 2013;31(31):3997–4013 10.1200/jco.2013.50.9984. [PubMed: 24101045]
39. Symmans WF, Peintinger F, Hatzis C, Rajan R, Kuerer H, Valero V, et al. Measurement of residual breast cancer burden to predict survival after neoadjuvant chemotherapy. J Clin Oncol 2007;25(28):4414–22 10.1200/jco.2007.10.6823. [PubMed: 17785706]
40. Silvestrini R, Veneroni S, Daidone MG, Benini E, Boracchi P, Mezzetti M, et al. The Bcl-2 protein: a prognostic indicator strongly related to p53 protein in lymph node-negative breast cancer patients. J Natl Cancer Inst 1994;86(7):499–504. [PubMed: 8133533]
41. Leek RD, Kaklamanis L, Pezzella F, Gatter KC, Harris AL. bcl-2 in normal human breast and carcinoma, association with oestrogen receptor-positive, epidermal growth factor receptor-negative tumours and in situ cancer. Br J Cancer 1994;69(1):135–9. [PubMed: 8286195]
42. Bhargava V, Kell DL, van de Rijn M, Warnke RA. Bcl-2 immunoreactivity in breast carcinoma correlates with hormone receptor positivity. Am J Pathol 1994;145(3):535–40. [PubMed: 8080038]

43. Shen K, Ma X, Zhu C, Wu X, Jia H. Safety and Efficacy of Trastuzumab Emtansine in Advanced Human Epidermal Growth Factor Receptor 2-Positive Breast Cancer: a Meta-analysis. Scientific reports 2016;6:23262 10.1038/srep23262. [PubMed: 26979925]
44. Gandhi L, Camidge DR, Ribeiro de Oliveira M, Bonomi P, Gandara D, Khaira D, et al. Phase I study of Navitoclax (ABT-263), a novel Bcl-2 family inhibitor, in patients with small-cell lung cancer and other solid tumors. J Clin Oncol 2011;29(7):909–16 10.1200/jco.2010.31.6208. [PubMed: 21282543]
45. Rudin CM, Hann CL, Garon EB, Ribeiro de Oliveira M, Bonomi PD, Camidge DR, et al. Phase II study of single-agent navitoclax (ABT-263) and biomarker correlates in patients with relapsed small cell lung cancer. Clin Cancer Res 2012;18(11):3163–9 10.1158/1078-0432.ccr-11-3090. [PubMed: 22496272]
46. Ogston KN, Miller ID, Payne S, Hutcheon AW, Sarkar TK, Smith I, et al. A new histological grading system to assess response of breast cancers to primary chemotherapy: prognostic significance and survival. Breast 2003;12(5):320–7. [PubMed: 14659147]
47. van Delft MF, Wei AH, Mason KD, Vandenberg CJ, Chen L, Czabotar PE, et al. The BH3 mimetic ABT-737 targets selective Bcl-2 proteins and efficiently induces apoptosis via Bak/Bax if Mcl-1 is neutralized. Cancer Cell 2006;10(5):389–99 10.1016/j.ccr.2006.08.027. [PubMed: 17097561]
48. Chen S, Dai Y, Harada H, Dent P, Grant S. Mcl-1 down-regulation potentiates ABT-737 lethality by cooperatively inducing Bak activation and Bax translocation. Cancer Res 2007;67(2):782–91 10.1158/0008-5472.can-06-3964. [PubMed: 17234790]
49. Xiao Y, Nimmer P, Sheppard GS, Bruncko M, Hessler P, Lu X, et al. MCL-1 Is a Key Determinant of Breast Cancer Cell Survival: Validation of MCL-1 Dependency Utilizing a Highly Selective Small Molecule Inhibitor. Mol Cancer Ther 2015;14(8):1837–47 10.1158/1535-7163.mct-14-0928. [PubMed: 26013319]
50. Leverson JD, Zhang H, Chen J, Tahir SK, Phillips DC, Xue J, et al. Potent and selective small-molecule MCL-1 inhibitors demonstrate on-target cancer cell killing activity as single agents and in combination with ABT-263 (navitoclax). Cell Death Dis 2015;6:e1590 10.1038/cddis.2014.561. [PubMed: 25590800]
51. Xiao C, Gong Y, Han EY, Gonzalez-Angulo AM, Sneige N. Stability of HER2-positive status in breast carcinoma: a comparison between primary and paired metastatic tumors with regard to the possible impact of intervening trastuzumab treatment. Ann Oncol 2011;22(7):1547–53 10.1093/annonc/mdq623. [PubMed: 21239403]
52. Niikura N, Liu J, Hayashi N, Mittendorf EA, Gong Y, Palla SL, et al. Loss of human epidermal growth factor receptor 2 (HER2) expression in metastatic sites of HER2-overexpressing primary breast tumors. J Clin Oncol 2012;30(6):593–9 10.1200/jco.2010.33.8889. [PubMed: 22124109]
53. Hurley J, Doliny P, Reis I, Silva O, Gomez-Fernandez C, Velez P, et al. Docetaxel, cisplatin, and trastuzumab as primary systemic therapy for human epidermal growth factor receptor 2-positive locally advanced breast cancer. J Clin Oncol 2006;24(12):1831–8 10.1200/jco.2005.02.8886. [PubMed: 16549824]
54. Hirata T, Shimizu C, Yonemori K, Hirakawa A, Kouno T, Tamura K, et al. Change in the hormone receptor status following administration of neoadjuvant chemotherapy and its impact on the long-term outcome in patients with primary breast cancer. Br J Cancer 2009;101(9):1529–36 10.1038/sj.bjc.6605360. [PubMed: 19809429]
55. Mittendorf EA, Wu Y, Scaltriti M, Meric-Bernstam F, Hunt KK, Dawood S, et al. Loss of HER2 amplification following trastuzumab-based neoadjuvant systemic therapy and survival outcomes. Clin Cancer Res 2009;15(23):7381–8 10.1158/1078-0432.ccr-09-1735. [PubMed: 19920100]
56. Guarneri V, Dieci MV, Barbieri E, Piacentini F, Omarini C, Ficarra G, et al. Loss of HER2 positivity and prognosis after neoadjuvant therapy in HER2-positive breast cancer patients. Ann Oncol 2013;24(12):2990–4 10.1093/annonc/mdt364. [PubMed: 24013581]
57. Parinyanitikul N, Lei X, Chavez-MacGregor M, Liu S, Mittendorf EA, Litton JK, et al. Receptor status change from primary to residual breast cancer after neoadjuvant chemotherapy and analysis of survival outcomes. Clin Breast Cancer 2015;15(2):153–60 10.1016/j.clbc.2014.09.006. [PubMed: 25454687]

58. Jin X, Jiang YZ, Chen S, Yu KD, Shao ZM, Di GH. Prognostic value of receptor conversion after neoadjuvant chemotherapy in breast cancer patients: a prospective observational study. Oncotarget 2015;6(11):9600–11 10.18632/oncotarget.3292. [PubMed: 25826079]
59. Lim SK, Lee MH, Park IH, You JY, Nam BH, Kim BN, et al. Impact of Molecular Subtype Conversion of Breast Cancers after Neoadjuvant Chemotherapy on Clinical Outcome. Cancer research and treatment : official journal of Korean Cancer Association 2016;48(1):133–41 10.4143/crt.2014.262. [PubMed: 25865655]
60. Jones RL, Lakhani SR, Ring AE, Ashley S, Walsh G, Smith IE. Pathological complete response and residual DCIS following neoadjuvant chemotherapy for breast carcinoma. Br J Cancer 2006;94(3):358–62 10.1038/sj.bjc.6602950. [PubMed: 16421590]
61. Mazouni C, Peintinger F, Wan-Kau S, Andre F, Gonzalez-Angulo AM, Symmans WF, et al. Residual ductal carcinoma in situ in patients with complete eradication of invasive breast cancer after neoadjuvant chemotherapy does not adversely affect patient outcome. J Clin Oncol 2007;25(19):2650–5 10.1200/jco.2006.08.2271. [PubMed: 17602071]
62. Kan S, Koido S, Okamoto M, Hayashi K, Ito M, Kamata Y, et al. Gemcitabine treatment enhances HER2 expression in low HER2-expressing breast cancer cells and enhances the antitumor effects of trastuzumab emtansine. Oncol Rep 2015;34(1):504–10 10.3892/or.2015.3974. [PubMed: 25976081]
63. Zhang H, Nimmer PM, Tahir SK, Chen J, Fryer RM, Hahn KR, et al. Bcl-2 family proteins are essential for platelet survival. Cell death and differentiation 2007;14(5):943–51 10.1038/sj.cdd.4402081. [PubMed: 17205078]
64. Tse C, Shoemaker AR, Adickes J, Anderson MG, Chen J, Jin S, et al. ABT-263: a potent and orally bioavailable Bcl-2 family inhibitor. Cancer Res 2008;68(9):3421–8 10.1158/0008-5472.can-07-5836. [PubMed: 18451170]
65. Thon JN, Devine MT, Jurak Begonja A, Tibbitts J, Italiano JE Jr. High-content live-cell imaging assay used to establish mechanism of trastuzumab emtansine (T-DM1)--mediated inhibition of platelet production. Blood 2012;120(10):1975–84 10.1182/blood-2012-04-420968. [PubMed: 22665936]
66. Uppal H, Doudement E, Mahapatra K, Darbonne WC, Bumbaca D, Shen BQ, et al. Potential Mechanisms for Thrombocytopenia Development with Trastuzumab Emtansine (T-DM1). Clin Cancer Res 2015;21(1):123–33 10.1158/1078-0432.ccr-14-2093. [PubMed: 25370470]
67. Zhao H, Gulesserian S, Ganesan SK, Ou J, Morrison K, Zeng Z, et al. Inhibition of Megakaryocyte Differentiation by Antibody-Drug Conjugates (ADCs) is Mediated by Macropinocytosis: Implications for ADC-induced Thrombocytopenia. Mol Cancer Ther 2017;16(9):1877–86 10.1158/1535-7163.mct-16-0710. [PubMed: 28655784]
68. Dokter W, Ubink R, van der Lee M, van der Vleuten M, van Achterberg T, Jacobs D, et al. Preclinical profile of the HER2-targeting ADC SYD983/SYD985: introduction of a new duocarmycin-based linker-drug platform. Mol Cancer Ther 2014;13(11):2618–29 10.1158/1535-7163.mct-14-0040-t. [PubMed: 25189543]
69. van der Lee MM, Groothuis PG, Ubink R, van der Vleuten MA, van Achterberg TA, Loosveld EM, et al. The Preclinical Profile of the Duocarmycin-Based HER2-Targeting ADC SYD985 Predicts for Clinical Benefit in Low HER2-Expressing Breast Cancers. Mol Cancer Ther 2015;14(3):692–703 10.1158/1535-7163.mct-14-0881-t. [PubMed: 25589493]
70. Yao X, Jiang J, Wang X, Huang C, Li D, Xie K, et al. A novel humanized anti-HER2 antibody conjugated with MMAE exerts potent anti-tumor activity. Breast Cancer Res Treat 2015;153(1):123–33 10.1007/s10549-015-3503-3. [PubMed: 26253944]
71. Ogitani Y, Aida T, Hagihara K, Yamaguchi J, Ishii C, Harada N, et al. DS-8201a, a novel HER2-targeting ADC with a novel DNA topoisomerase I inhibitor, demonstrates a promising anti-tumor efficacy with differentiation from T-DM1. Clin Cancer Res 2016 10.1158/1078-0432.ccr-15-2822.
72. Li JY, Perry SR, Muniz-Medina V, Wang X, Wetzel LK, Rebelatto MC, et al. A Biparatopic HER2-Targeting Antibody-Drug Conjugate Induces Tumor Regression in Primary Models Refractory to or Ineligible for HER2-Targeted Therapy. Cancer Cell 2016;29(1):117–29 10.1016/j.ccell.2015.12.008. [PubMed: 26766593]

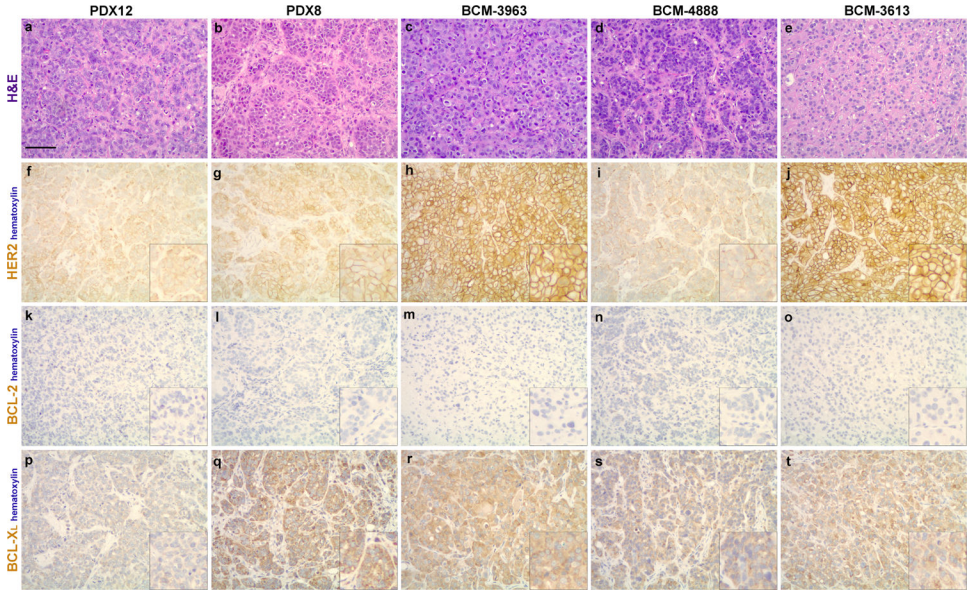

Figure 1.

Comparison of HER2, BCL-2 and BCL-X_L expression levels. Tumor sections were visualized via H&E (**a–e**) and were evaluated for HER2 (**f–j**), BCL-2 (**k–o**) and BCL-X_L (**p–t**) via IHC. Representative IHC images are presented for PDX12, PDX8, BCM-3963, BCM-4888 and BCM-3613. IHC or H-scores for each marker are summarized in Table 1. Scale bar, ~90 μm.

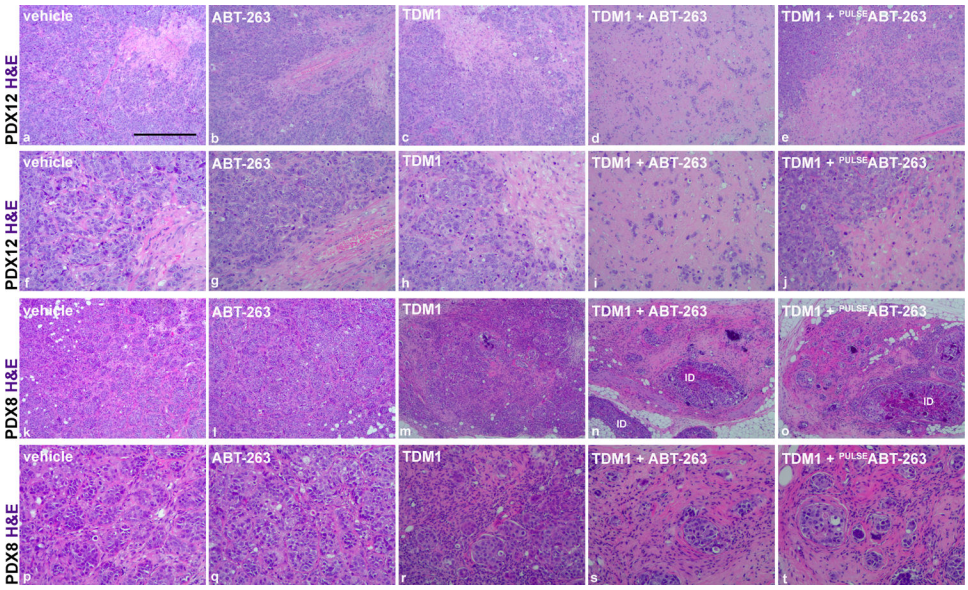

Figure 2.

Microscopic analysis of treatment effects. Representative H&E images are presented to compare PDX12 (**a–j**) and PDX8 (**k–t**) treatment groups. Note significant elimination of tumor cells post combination treatment (**d** and **n** or **i** and **s)**. H&E images presented in **a–e** and **k–o** are magnified in **f–j** and **p–t**, respectively. The presence of notable intraductal carcinoma (ID) is indicated. Scale bar, ~480 μm.

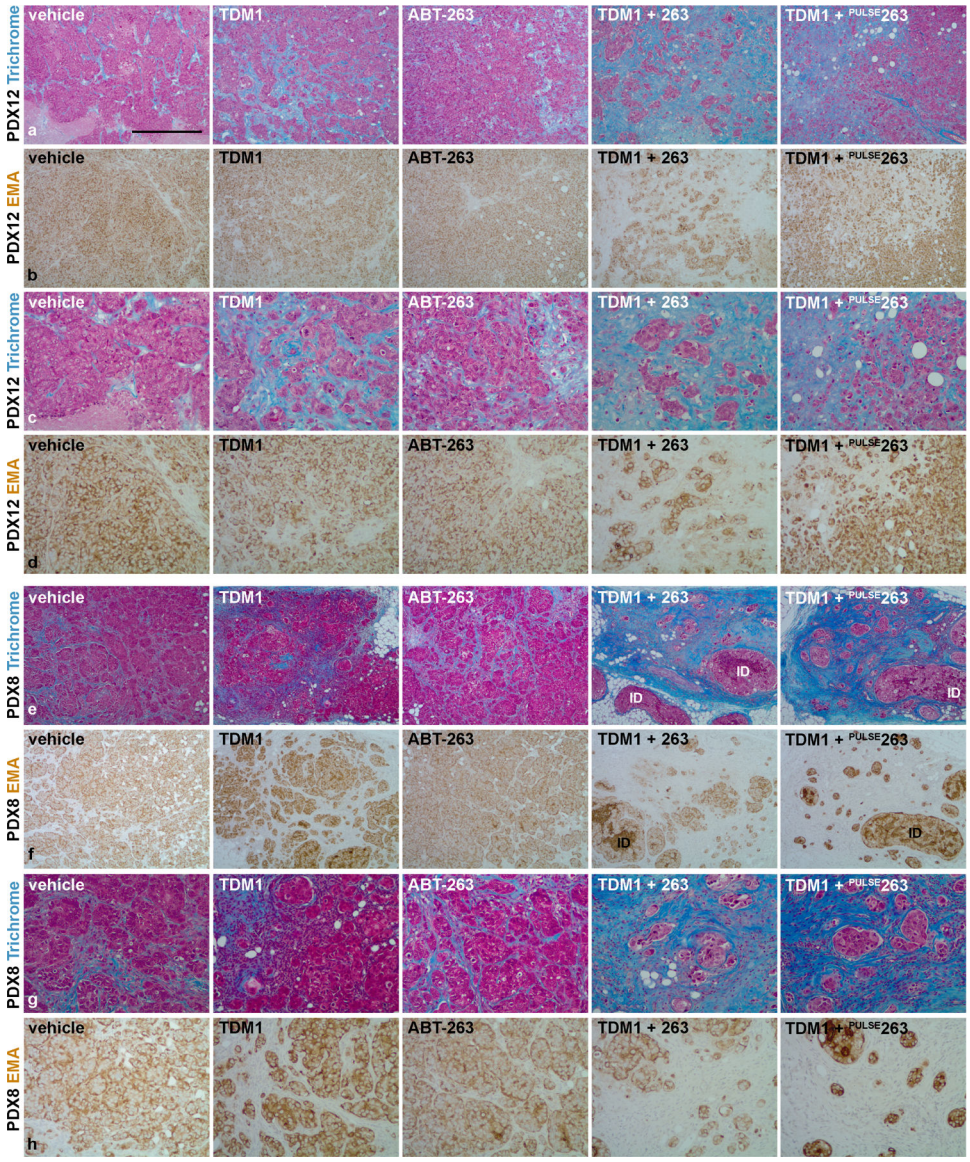

Figure 3.

Tumor cellular and stromal characterization post-treatment. Representative Masson's trichrome stained tumor sections from PDX12 (**a** and **c**) and PDX8 (**e** and **g**) comparing vehicle controls, single agents and combination treatment. Masson's trichrome stains the cell nuclei (black), cell cytoplasm (red) and collagen (blue). Note the emergence of scar-like reactive stroma at the tumor bed in response to combination treatment (**c** and **g**). Representative EMA stained tumor sections from PDX12 (**b** and **d**) and PDX8 (**f** and **h**) comparing treatment groups. Note the substantial elimination of invasive tumor cells in response to combination treatment (**d** and **h**). The elimination of invasive tumor cells and the emergence of a desmoplastic stroma are characteristic features of effective treatment response. The images presented in **a** and **b** or **e** and **f** are magnified in **c** and **d** or **g** and **h**, respectively. The presence of notable intraductal carcinoma (ID) is indicated. Scale bar, ~525 μm.

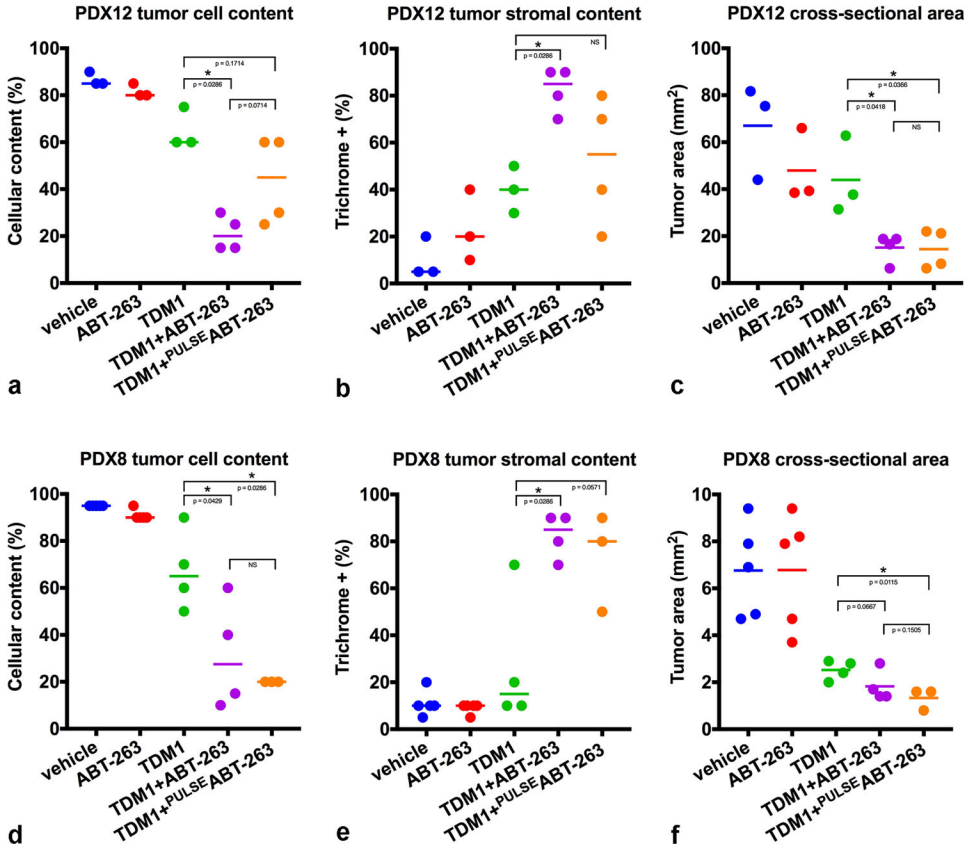

Figure 4.

Quantitative pathological assessment of treatment effects. Tumor cellular content was summarized across multiple tumors from PDX12 (**a**) and PDX8 (**d**) experiments (Mann-Whitney one-tail test PDX12: T-DM1 versus T-DM1 + ABT-263; *p* value = 0.0286, T-DM1 versus T-DM1 + ^{PULSE}ABT-263; *p* value = 0.1714 and PDX8: T-DM1 versus T-DM1 + ABT-263; *p* value = 0.0429, T-DM1 versus T-DM1 + ^{PULSE}ABT-263; *p* value = 0.0286). Tumor stromal content was summarized across multiple tumors from PDX12 (**b**) and PDX8 (**e**) experiments (Mann-Whitney one-tail test PDX12: T-DM1 versus T-DM1 + ABT-263; *p* value = 0.0286, T-DM1 versus T-DM1 + ^{PULSE}ABT-263; *p* value = NS and PDX8: T-DM1 versus T-DM1 + ABT-263; *p* value = 0.0286, T-DM1 versus T-DM1 + ^{PULSE}ABT-263; *p* value = 0.0571). Tumor cross-sectional area was summarized across multiple tumors from PDX12 (**c**) and PDX8 (**f**) experiments (Welch's one-tail *t* test PDX12: T-DM1 versus T-DM1 + ABT-263; *p* value = 0.0418, T-DM1 versus T-DM1 + ^{PULSE}ABT-263; *p* value = 0.0366 and PDX8: T-DM1 versus T-DM1 + ABT-263; *p* value = 0.0667, T-DM1 versus T-DM1 + ^{PULSE}ABT-263; *p* value = 0.0115). *p* values ≤ 0.05 (*) are indicated as numerical values, *p* values > 0.05 and ≤ 0.2 are also indicated as numerical values whereas *p* values > 0.2 are indicated as NS. Additional statistical tests comparing vehicle with each of the treatment groups are summarized in Supplementary Table 2. Each line represents the median (**a** and **d** or **b** and **e**) or the mean (**c** and **f**).

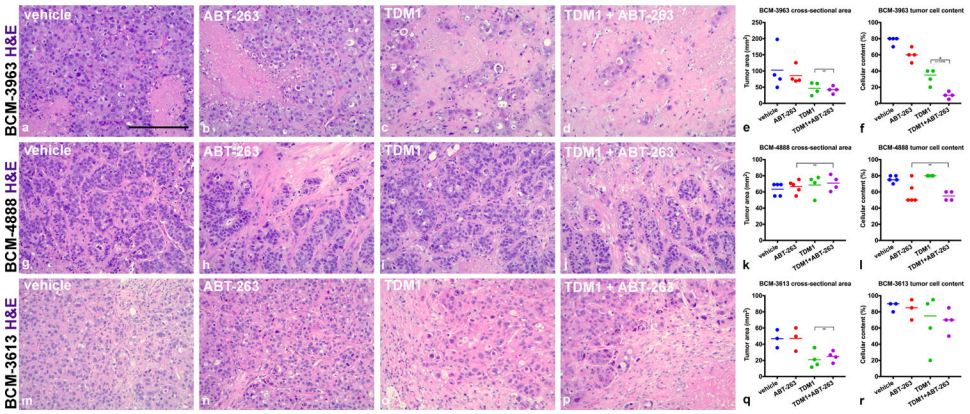

Figure 5.

BCM-3963, BCM-4888 and BCM-3613 response to combination treatment. BCM tumors were administered vehicle controls, single agents or combination treatments for 14 days. ABT-263 was administered continuously days 1–14. Representative H&E images are presented to compare BCM-3963 (**a–d**), BCM-4888 (**g–j**) and BCM-3613 (**m–p**) treatment groups. Note significant elimination of BCM-3963 tumor cells post-combination treatment (**d**). Tumor cross-sectional area was summarized across multiple tumors from BCM-3963 (**e**), BCM-4888 (**k**) and BCM-3613 (**q**) experiments (Welch's one-tail *t* test BCM-3613: vehicle versus T-DM1; *p* value = 0.0159). Tumor cellular content was summarized across multiple tumors from BCM-3963 (**f**), BCM-4888 (**l**) and BCM-3613 (**r**) experiments (Mann-Whitney one-tail test BCM-3963: vehicle versus T-DM1; *p* value = 0.0143, T-DM1 versus T-DM1 + ABT-263; *p* value = 0.0143 and BCM-4888: vehicle versus ABT-263; *p* value = 0.0357). *p* values ≤ 0.05 (*) are indicated as numerical values and *p* values > 0.2 are indicated as NS. Additional statistical tests comparing vehicle with each of the treatment groups are summarized in Supplementary Table 3. Each line represents the mean (**e, k** and **q**) or the median (**f, l** and **r**). Scale bar, ~185 μm.

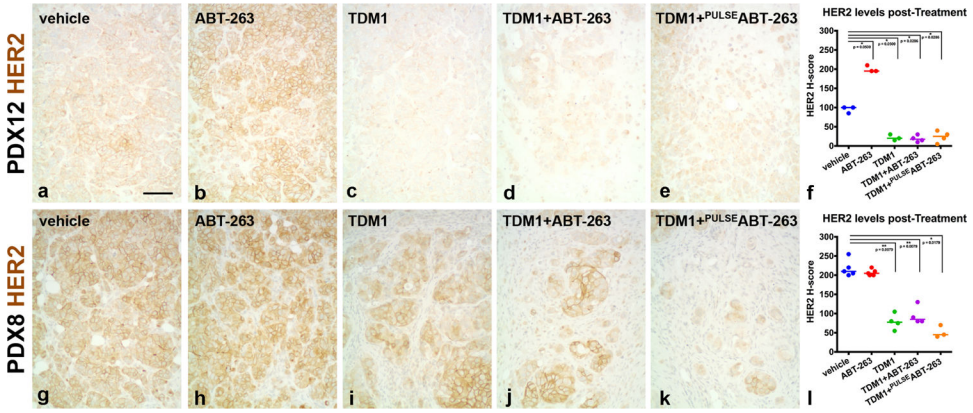

Figure 6.

HER2 levels post-treatment. PDX12 (**a–e**) and PDX8 (**g–k**) tumor sections were evaluated for HER2 via IHC. Representative HER2 IHC images are presented to compare treatment groups. Note PDX12 and PDX8 T-DM1-treated tumors express lower levels of HER2 (**c–e** and **i–k**). Note single agent ABT-263 upregulates HER2 in PDX12 tumors (**b**). HER2 was quantified via H-score assessment (37). Data were summarized across multiple tumors from PDX12 (**f**) and PDX8 (**l**) experiments (Mann-Whitney one-tail test PDX12: vehicle versus ABT-263; p value = 0.0500, vehicle versus T-DM1; p value = 0.0500, vehicle versus T-DM1 + ABT-263; p value = 0.0286, vehicle versus T-DM1 + ^{PULSE}ABT-263; p value = 0.0286 and PDX8: vehicle versus T-DM1; p value = 0.0079, vehicle versus T-DM1 + ABT-263; p value = 0.0079, vehicle versus T-DM1 + ^{PULSE}ABT-263; p value = 0.0179). p values ≤ 0.05 (*) or ≤ 0.01 (**) are indicated as numerical values. Each line represents the median. Scale bar, ~90 μm.

Table 1.

Characterization of PDX models

PDX	PATIENT tumor source (34,35)[1]	PATIENT clinical treatments (34,35)[2]	HER2 IHC-score	ER Status[3]	BCL-2 H-score[4]	BCL-X_L H-score[4]
PDX12	post-T× PE	cape; vino; trastuzumab; lapatinib	1+	−	0	97
PDX8	post-T× PE	5-FU; cape	2+	−	0	183
BCM-3963	pre-T× PT	NONE	3+	−	0	110
BCM-4888	post-T× PT	cyclo; doxo; GSI	2+	+	13	102
BCM-3613	post-T× PE	cyclo; doxo; pacl; trastuzumab; lapatinib; GSI; doce; others	3+	−	0	117

[1] T×, treatment; PE, pleural effusion; PT, primary breast tumor

[2] cape, capecitabine; vino, vinorelbine; 5-FU, 5-fluorouracil; cyclo, cyclophosamide; doxo, doxorubicin; GSI, gamma secretase inhibitor; pacl, paclitaxel; doce, docetaxel

[3] ER -positive (+) or -negative (−) as previously described (34,35)

[4] H-score represents the average of 3–5 tumors per PDX